Nonlinear Analysis: Modelling and Control, Vol. 27, No. 4, 684–699
https://doi.org/10.15388/namc.2022.27.26741

Vilnius University Press

Effects of Joule heating, thermal radiation on MHD pulsating flow of a couple stress hybrid nanofluid in a permeable channel

Somasundaram Rajamani, Anala Subramanyam Reddy[1]

Department of Mathematics, School of Advanced Sciences,
Vellore Institute of Technology, Vellore-632014, India
anala.subramanyamreddy@gmail.com

Received: June 4, 2021 / **Revised:** December 29, 2021 / **Published online:** April 13, 2022

Abstract. The current work deals with the pulsatile hydromagnetic flow of blood-based couple stress hybrid nanofluid in a porous channel. For hybrid nanofluid, the fusion of gold (Au) and copper oxide (CuO) nanoparticles are suspended to the blood (base fluid). In this model, the employment of viscous dissipation, radiative heat, and Ohmic heating is incorporated. The governing flow equations (set of partial differential equations) are modernized to set of ordinary differential equations by using the perturbation technique. The nondimensional governing equations are solved by adopting the shooting procedure with the help of the Runge–Kutta fourth-order approach. Temperature distributions of hybrid nanofluid and conventional mono nanofluids are portrayed via pictorial results to claim that the hybrid nanofluid has better temperature distribution than mono nanofluids. Temperature is raising for the magnifying viscous dissipation, whereas the reverse behavior can be found with a rise in couple stress parameter. The heat transfer rate is getting high for the higher values of the Eckert number, and the same behavior is noticed with the uplifting magnetic field.

Keywords: pulsatile flow, porous channel, couple stress hybrid nanofluid, Joule heating, thermal radiation.

1 Introduction

For the prominent benefits in the study of blood flow and other industrial treatments, it is far-reaching to explore the pulsatile flow. Notable awareness augmented on the pulsatile phenomena attributable to its episode in many physiological cum medical processes and its potential essence in next-generation smart mechanisms [16,31]. Rana and Murthy [18] assessed the influence of pulsatile pressure gradient in the standardized solute dispersion for a non-Newtonian fluid. The flow of pulsating nature of blood as a non-Newtonian model in a narrow tapered channel schematized by Sankar [21]. Vijayalakshmi et al. [30]

[1]Corresponding author.

worked on the perturbation mechanism to get the rational results for the pulsating flow of magnetohydrodynamic nanofluid with thermal radiation. In addition, authors given special attention to study the thermophysical behavior of silver, copper oxide, alumina, and titania nanoparticles by evaluating the graphical outcomes of the corresponding temperature and heat transfer rate profiles. Qomi et al. [15] investigated the novel problem of pulsating flow of hybrid nanofluid with the effect of applied magnetic field simultaneously in a microchannel. Shawky [23] investigated the heat transfer on the pulsatile flow of dusty non-Newtonian fluid with the presence of applied magnetic field and Joule heating by using Lightill method with the support of perturbation technique. Venkatesan and Reddy [29] analytically investigated the pulsatile flow of a non-Newtonian Oldroyd-B nanofluid through a channel with Ohmic heating, viscous dissipation, and thermal radiation by adopting the perturbation method. Recently, Ye et al. [32] comprehensively reviewed the latest research status of pulsating flow on heat transfer phenomenon. Here the authors summarized that the manufacturing, chemical engineering, thermal engineering, biomedical engineering, and electronic engineering are having great need of the study concerned with enhancing heat transfer properties of pulsatile flow.

The thermal conductivity of nanoparticles helped to enhance the lower thermal conductivity of base fluids, which is named as nanofluids addressed by Choi and Eastman [4]. These innovative heat transfer fluids have enormous thermal absorption/eviction applications in industries as well as day-to-day life [3, 8, 19]. Hatami et al. [9] aced the flow of a non-Newtonian blood-gold nanofluid in a permeable channel with the presence of magnetic effect by utilizing numerical and analytical investigations. Exclamatory outcomes in heat transfer demands and the outlandish behavior of nanofluids accelerate us to the next generation of nanofluids, by fusing more than one dissimilar nanoparticles in a base fluid, to get the additive effects of those nanoparticles for the enrichment in heat transfer of base fluids, this next step of nanofluids is known as hybrid nanofluids. Hybrid nanofluids are planned to further enhancement in heat transfer than mono nanofluids such as overcoming the defectivity of heat transfer in certain situations of conventional ones and improve the heat transfer rate in applications of single nanoparticle suspended base fluid [20, 22]. Devi and Devi [7] numerically studied the course of a hybrid nanofluid over an expanding sheet with the upshots of suction and magnetic parameters. Hussain et al. [10] inspected the flow of a hydromagnetic hybrid nanofluid in an open cavity with a horizontal channel by employing various numerical techniques. Ahmed and Xu [2] analytically examined the unsteady pulsating flow of copper-alumina-water hybrid nanofluid driven in a microchannel with the consideration of magnetic parameter and thermal radiation effects. Muneeshwaran et al. [14] done a review on the role of hybrid nanofluid on thermal transport phenomenon. Here the authors claimed that the thermal conductivity of hybrid nanofluid is the reason behind for the increment in heat transfer rate, and the thermophysical properties are the main factors that affect the stability of hybrid nanoparticles.

To understand the flow behavior of many real-life fluids taken part in calamity situations and vast industrial applications, the knowledge of non-Newtonian fluids is mattered to us. Couple stress fluids are the desirable kind of non-Newtonian fluids due to their help to get the schematic blueprint of the flow behavior of biofluids such as blood, synovial

fluid [6, 26]. The motif of couple stress theory proposed by Stokes [27] by modeling the mechanical interactions of fluid particles on the root of continuum concept. Adesanya and Makinde [1] analyzed the pressure-driven flow of a couple stress fluid with the employment of magnetic parameter and thermal radiation by utilizing the Adomian decomposition method. Tripathi et al. [28] modeled the flow of couple stress hybrid nanofluid and claimed that their model is dedicated to drug delivery and smart-peristaltic mechanisms. Rajamani and Reddy [17] analytically studied the magnetohydrodynamic pulsatile flow of a couple stress nanofluid via channel with the presence of Joule heating and radiative heat by using the perturbation technique. Here the authors validated their results with the comparison of outcomes from perturbation technique and Runge–Kutta 4th order scheme with the support of shooting technique. Recently, Jawad et al. [11] have carried out an analytical investigation for the couple stress hybrid nanofluid flow past a permeable sheet with the presence of magnetic field, Brownian motion, thermophoresis, heat source, and thermal radiation. Here the authors considered the couple stress hybrid nanoparticles as a targeted drug carrier that can be utilized in the biomedicine fields in the drug delivery system.

In the light of promising benefits in engineering and industries, like power generation, space devices, polymer processing, electrical and electronic devices [5, 25], there is a lot to discuss about Joule heating, thermal radiation, and viscous dissipation effects. Zaib and Shafie [33] investigated the unsteady flow of electrically treated fluid past an expanding sheet with the episodes of thermal radiation, viscous dissipation, and Joule heating. Kumar et al. [13] studied the pulsating flow of MHD Casson nanofluid in a vertical permeable space. Here the impacts of Ohmic and viscous dissipations are taken into account. An inspection for the radiative heat on the flow of non-Newtonian fluid in a penetrable medium with effects of heat source/sink and the magnetic parameter was done by Khedr et al. [12]. Sreedevi et al. [24] analyzed the thermal radiation for the unsteady hybrid nanofluid flow with the effects of magnetic and suction parameters.

In this study, a numerical study of MHD pulsatile flow of electrically treated couple stress hybrid nanofluid in a penetrable channel with the influences of Joule heating and thermal radiation is inspected. Hybrid nanoparticles are the fusion of gold and copper oxide nanoparticles. Blood is considered as the electrically conducting base fluid due to influencing applications not only in the bio-medical field but also in industries. The dynamics of blood flow is analyzed for hybrid nanofluid and the conventional mono nanofluids with the variations of emerging parameters that are involved in the current analysis. There is an enhancement in temperature distribution and the rate of heat transfer while using hybrid nanofluid than the mono nanofluids, which is presented via pictorial results.

2 Formulation of the problem

Consider an electrically conducting pulsating flow of a couple stress hybrid nanofluid in a permeable channel. In this study, for hybrid nanofluid, the fusion of gold and copper oxide nanoparticles are taken as nanoparticles, and the blood is chosen as base fluid. The clouts of thermal radiation, viscous dissipation, and Ohmic heating are considered into account.

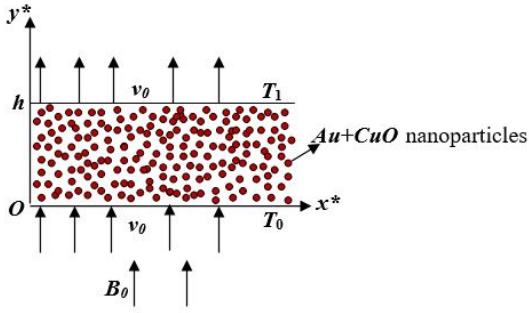

Figure 1. Flow model of the problem.

The flow model of the current study is presented in Fig. 1. Let us assume that the bottom wall coincides with the x^*-axis, while the y^*-axis is normal to it. An applied magnetic field of magnitude B_0 is entreated uniformly orthogonal to both walls. T_1 and T_0 are the wall temperatures of upper and lower walls, respectively ($T_0 < T_1$), and h is the distance between the walls. The fluid is injected through the bottom wall with a velocity v_0 and sucked out from the top wall at the same rate. The constitutive equations concerning the force stress t_{ij} and the rate of deformation tensor d_{ij} are given by [6, 27]

$$t_{ij} = -p\delta_{ij} + \lambda \operatorname{div}(\bar{q})\delta_{ij} + 2\mu d_{ij} - \frac{1}{2}\varepsilon_{ijk}[m_k + 4\eta\omega_{k,rr} + \rho c_k],$$
$$m_{ij} = \frac{1}{3}m\delta_{ij} + 4\eta\omega_{j,i} + 4\eta'\omega_{i,j}.$$

The couple stress tensor m_{ij} that arises in the theory has the linear constitutive relation. In the above, $\omega = \operatorname{curl}(\bar{q})/2$ is the spin vector, $\omega_{i,j}$ is the spin tensor, m is the trace of couple stress tensor m_{ij}, p is the fluid pressure, and ρc_k is the body couple vector. These material constants are constrained by the inequalities

$$\mu \geqslant 0, \qquad 3\lambda + 2\mu \geqslant 0, \qquad \eta \geqslant 0, \qquad |\eta'| \leqslant \eta.$$

Assume that the flow is induced by a pressure gradient, which is taken by [16, 31]

$$-\frac{1}{\rho_f}\frac{\partial P^*}{\partial x^*} = A\big(1 + \varepsilon \mathrm{e}^{\mathrm{i}\omega t^*}\big), \tag{1}$$

here P^* is the fluid pressure, ω is the frequency, A is a constant, t^* is time, and ε ($\ll 1$) is a positive quantity. Under these hypotheses the governing equations of the current flow are

$$\rho_{hnf}\left[\frac{\partial u^*}{\partial t^*} + v_0\frac{\partial u^*}{\partial y^*}\right] = -\frac{\partial P^*}{\partial x^*} + \mu_{hnf}\left(\frac{\partial^2 u^*}{\partial y^{*2}}\right) - \eta\frac{\partial^4 u^*}{\partial y^{*4}} - \sigma_{hnf}{B_0}^2 u^*, \tag{2}$$

$$(\rho C_p)_{hnf}\left[\frac{\partial T^*}{\partial t^*} + v_0\frac{\partial T^*}{\partial y^*}\right] = k_{hnf}\frac{\partial^2 T^*}{\partial y^{*2}} + \mu_{hnf}\left(\frac{\partial u^*}{\partial y^*}\right)^2 + \eta\left(\frac{\partial^2 u^*}{\partial y^{*2}}\right)^2 - \frac{\partial q_r^*}{\partial y^*} + Q_0(T^* - T_0) + \sigma_{hnf}B_0^2 u^{*2}. \tag{3}$$

Here u^* is the velocity along the x^*-direction, ρ_{hnf}, μ_{hnf}, $(\rho Cp)_{hnf}$, k_{hnf}, and σ_{hnf} represent density, dynamic viscosity, effective specific heat, thermal conductivity, and electrical conductivity of hybrid nanofluid, respectively, and the subscripts hnf, nf, f, and s denote hybrid nanofluid, nanofluid, base fluid (blood), and solid nanoparticles, respectively. T^* is the temperature of hybrid nanofluid, η is coefficient of couple stress viscosity, Q_0 is coefficient of heat source/sink, and the radiative heat flux is denoted as q_r^*.

The related boundary conditions (BCs) are

$$u^*(0)=0, \qquad \frac{\partial^2 u^*}{\partial y^{*2}}(0)=0, \qquad T^*(0)=T_0,$$
$$u^*(h)=0, \qquad \frac{\partial^2 u^*}{\partial y^{*2}}(h)=0, \qquad T^*(h)=T_1.$$

The thermal characteristics of blood, Au and CuO nanoparticles are specified in Table 1. The physical features of nanofluid and hybrid nanofluid are defined as [7, 10, 22]

$$\begin{aligned}
(\rho Cp)_{nf} &= (1-\phi)(\rho Cp)_f + \phi(\rho Cp)_s,\\
\mu_{nf} &= \frac{\mu_f}{(1-\phi)^{2.5}}, \qquad \rho_{nf} = (1-\phi)\rho_f + \phi\rho_s,\\
\frac{k_{nf}}{k_f} &= \frac{k_s+2k_f-2\phi(k_f-k_s)}{k_s+2k_f+\phi(k_f-k_s)}, \qquad \frac{\sigma_{nf}}{\sigma_f} = 1+\frac{3(\frac{\sigma_s}{\sigma_f}-\phi)}{(\frac{\sigma_s}{\sigma_f}+2)-(\frac{\sigma_s}{\sigma_f}-1)\phi};
\end{aligned}$$

$$\begin{aligned}
(\rho Cp)_{hnf} &= (1-\phi)(\rho Cp)_f + \phi_{\text{Au}}(\rho Cp)_{\text{Au}} + \phi_{\text{CuO}}(\rho Cp)_{\text{CuO}},\\
\mu_{hnf} &= \frac{\mu_f}{(1-(\phi_{\text{Au}}+\phi_{\text{CuO}}))^{2.5}}, \qquad \rho_{hnf} = (1-\phi)\rho_f + \phi_{\text{Au}}\rho_{\text{Au}} + \phi_{\text{CuO}}\rho_{\text{CuO}},\\
\frac{k_{hnf}}{k_f} &= \frac{(\frac{\phi_{\text{Au}}k_{\text{Au}}+\phi_{\text{CuO}}k_{\text{CuO}}}{\phi})+2k_f+2(\phi_{\text{Au}}k_{\text{Au}}+\phi_{\text{CuO}}k_{\text{CuO}})-2\phi k_f}{(\frac{\phi_{\text{Au}}k_{\text{Au}}+\phi_{\text{CuO}}k_{\text{CuO}}}{\phi})+2k_f-(\phi_{\text{Au}}k_{\text{Au}}+\phi_{\text{CuO}}k_{\text{CuO}})+\phi k_f},\\
\frac{\sigma_{hnf}}{\sigma_f} &= 1+\frac{3(\frac{\phi_{\text{Au}}\sigma_{\text{Au}}+\phi_{\text{CuO}}\sigma_{\text{CuO}}}{\sigma_f}-\phi)}{(\frac{\phi_{\text{Au}}\sigma_{\text{Au}}+\phi_{\text{CuO}}\sigma_{\text{CuO}}}{\phi\sigma_f}+2)-(\frac{\phi_{\text{Au}}\sigma_{\text{Au}}+\phi_{\text{CuO}}\sigma_{\text{CuO}}}{\sigma_f}-\phi)}.
\end{aligned}$$

Here $\phi=\phi_{\text{Au}}+\phi_{\text{CuO}}$, ϕ is the volume fraction of nanoparticles.

By adopting the Rosseland approximation for the radiative heat flux (q_r^*), Eq. (3) becomes

$$\begin{aligned}
(\rho C_p)_{hnf}\left[\frac{\partial T^*}{\partial t^*}+v_0\frac{\partial T^*}{\partial y^*}\right] &= k_{hnf}\frac{\partial^2 T^*}{\partial y^{*2}}+\mu_{hnf}\left(\frac{\partial u^*}{\partial y^*}\right)^2+\eta\left(\frac{\partial^2 u^*}{\partial y^{*2}}\right)^2\\
&\quad+\frac{16}{3}\frac{\sigma^* T_1^3}{k^*}\frac{\partial^2 T^*}{\partial y^{*2}}+Q_0(T^*-T_0)+\sigma_{hnf}B_0^2 u^{*2}. \quad (4)
\end{aligned}$$

Here k^* is the Rosseland mean absorption coefficient, and σ^* is the Stephen–Boltzmann constant.

Table 1. The thermophysical properties of nanoparticles and blood [3, 19].

Property	Au	CuO	Blood
$\sigma\,[(\Omega\,\mathrm{m})^{-1}]$	$4.10 \cdot 10^{7}$	$2.7 \cdot 10^{-8}$	0.8
$\rho\,[\mathrm{kg/m^3}]$	19282	6500	1050
$k\,[\mathrm{W/mK}]$	310	18	0.52
$C_p\,[\mathrm{J/kg\,K}]$	129	540	3617

Now, with the help of the ensuing nondimensional parameters,

$$x^* = xh, \qquad y^* = yh, \qquad t^* = \frac{t}{\omega}, \qquad u^* = \frac{Au}{\omega},$$
$$P^* = \rho_f P A h, \qquad T^* = T_0 + \theta(T_1 - T_0),$$
$$H = \frac{\sqrt{\omega}h}{\sqrt{\upsilon_f}}, \qquad M = B_0 h\sqrt{\frac{\sigma_f}{\mu_f}}, \qquad Pr = \frac{\upsilon_f(\rho Cp)_f}{k_f}, \qquad Ec = \frac{A^2}{\omega^2(C_p)_f(T_1 - T_0)},$$
$$R = \frac{v_0 h}{\upsilon_f}, \qquad Rd = \frac{4\sigma^* {T_1}^3}{k^* k_f}, \qquad \lambda = \frac{\eta}{\mu_f h^2}, \qquad Q = \frac{Q_0 h^2}{\upsilon_f(\rho Cp)_f}.$$

Equations (1), (2), and (4) become

$$-\frac{\partial P}{\partial x} = 1 + \varepsilon \mathrm{e}^{\mathrm{i}t}, \tag{5}$$
$$A_1\left[\frac{\partial u}{\partial t} + \frac{R}{H^2}\frac{\partial u}{\partial y}\right] = -\frac{\partial P}{\partial x} + \frac{A_2}{H^2}\left(\frac{\partial^2 u}{\partial y^2}\right) - \frac{\lambda}{H^2}\frac{\partial^4 u}{\partial y^4} - \frac{A_5 M^2}{H^2}u, \tag{6}$$
$$A_3\left[\frac{\partial \theta}{\partial t} + \frac{R}{H^2}\frac{\partial \theta}{\partial y}\right] = \frac{(A_4 + \frac{4}{3}Rd)}{PrH^2}\left(\frac{\partial^2 \theta}{\partial y^2}\right) + \frac{A_2 Ec}{H^2}\left(\frac{\partial u}{\partial y}\right)^2 + \frac{\lambda Ec}{H^2}\left(\frac{\partial^2 u}{\partial y^2}\right)^2 + \frac{A_5 Ec M^2}{H^2}u^2 + \frac{Q}{H^2}\theta. \tag{7}$$

Here

$$A_1 = (1-\phi) + \phi_{\mathrm{Au}}\frac{\rho_{\mathrm{Au}}}{\rho_f} + \phi_{\mathrm{CuO}}\frac{\rho_{\mathrm{CuO}}}{\rho_f}, \qquad A_2 = \frac{1}{(1-(\phi_{\mathrm{Au}} + \phi_{\mathrm{CuO}}))^{2.5}},$$
$$A_3 = (1-\phi) + \phi_{\mathrm{Au}}\frac{(\rho Cp)_{\mathrm{Au}}}{(\rho Cp)_f} + \phi_{\mathrm{CuO}}\frac{(\rho Cp)_{\mathrm{CuO}}}{(\rho Cp)_f},$$
$$A_4 = \frac{(\frac{\phi_{\mathrm{Au}}k_{\mathrm{Au}} + \phi_{\mathrm{CuO}}k_{\mathrm{CuO}}}{\phi}) + 2k_f + 2(\phi_{\mathrm{Au}}k_{\mathrm{Au}} + \phi_{\mathrm{CuO}}k_{\mathrm{CuO}}) - 2\phi k_f}{(\frac{\phi_{\mathrm{Au}}k_{\mathrm{Au}} + \phi_{\mathrm{CuO}}k_{\mathrm{CuO}}}{\phi}) + 2k_f - (\phi_{\mathrm{Au}}k_{\mathrm{Au}} + \phi_{\mathrm{CuO}}k_{\mathrm{CuO}}) + \phi k_f},$$
$$A_5 = 1 + \frac{3(\frac{\phi_{\mathrm{Au}}\sigma_{\mathrm{Au}} + \phi_{\mathrm{CuO}}\sigma_{\mathrm{CuO}}}{\sigma_f} - \phi)}{(\frac{\phi_{\mathrm{Au}}\sigma_{\mathrm{Au}} + \phi_{\mathrm{CuO}}\sigma_{\mathrm{CuO}}}{\phi\sigma_f} + 2) - (\frac{\phi_{\mathrm{Au}}\sigma_{\mathrm{Au}} + \phi_{\mathrm{CuO}}\sigma_{\mathrm{CuO}}}{\sigma_f} - \phi)},$$

where Ec is Eckert number, M is Hartmann number, Pr is Prandtl number, Q is heat source/sink parameter, H is frequency parameter, λ is couple stress parameter, R is the cross-flow Reynolds number, Rd is the radiation parameter.

The corresponding BCs are

$$u(0)=0, \qquad \frac{\partial^2 u}{\partial y^2}(0)=0, \qquad \theta(0)=0,$$
$$u(1)=0, \qquad \frac{\partial^2 u}{\partial y^2}(1)=0, \qquad \theta(1)=1.$$

3 Solution of the problem

Owing to Eq. (5), the solution locutions for u and θ can be taken as

$$u(y)=u_0(y)+\varepsilon u_1(y)\mathrm{e}^{\mathrm{i}t}, \tag{8}$$
$$\theta(y)=\theta_0(y)+\varepsilon\theta_1(y)\mathrm{e}^{\mathrm{i}t}. \tag{9}$$

By substituting Eqs. (5), (8) and (9) into the Eqs. (6)–(7) and then likening the coefficients of different powers of ε, one can get

$$\lambda\frac{\mathrm{d}^4u_0}{\mathrm{d}y^4}-A_2\frac{\mathrm{d}^2u_0}{\mathrm{d}y^2}+A_1R\frac{\mathrm{d}u_0}{\mathrm{d}y}+A_5M^2u_0=H^2, \tag{10}$$
$$\lambda\frac{\mathrm{d}^4u_1}{\mathrm{d}y^4}-A_2\frac{\mathrm{d}^2u_1}{\mathrm{d}y^2}+A_1R\frac{\mathrm{d}u_1}{\mathrm{d}y}+\big(\mathrm{i}A_1H^2+A_5M^2\big)u_1=H^2, \tag{11}$$
$$\frac{1}{Pr}\left(A_4+\frac{4}{3}Rd\right)\frac{\mathrm{d}^2\theta_0}{\mathrm{d}y^2}-A_3R\frac{\mathrm{d}\theta_0}{\mathrm{d}y}+Q\theta_0+\lambda Ec\left(\frac{\mathrm{d}^2u_0}{\mathrm{d}y^2}\right)^2+A_2Ec\left(\frac{\mathrm{d}u_0}{\mathrm{d}y}\right)^2 + A_5EcM^2u_0^2=0, \tag{12}$$
$$\frac{1}{Pr}\left(A_4+\frac{4}{3}Rd\right)\frac{\mathrm{d}^2\theta_1}{\mathrm{d}y^2}-A_3R\frac{\mathrm{d}\theta_1}{\mathrm{d}y}+\big(Q-\mathrm{i}A_3H^2\big)\theta_1+2\lambda Ec\frac{\mathrm{d}^2u_0}{\mathrm{d}y^2}\frac{\mathrm{d}^2u_1}{\mathrm{d}y^2} + 2A_2Ec\frac{\mathrm{d}u_0}{\mathrm{d}y}\frac{\mathrm{d}u_1}{\mathrm{d}y}+2A_5EcM^2u_0u_1=0. \tag{13}$$

The corresponding BCs are

$$\begin{aligned} &u_0(0)=0, \quad u_1(0)=0, \quad \frac{\mathrm{d}^2u_0}{\mathrm{d}y^2}(0)=0, \quad \frac{\mathrm{d}^2u_1}{\mathrm{d}y^2}(0)=0,\\ &\theta_0(0)=0, \quad \theta_1(0)=0,\\ &u_0(1)=0, \quad u_1(1)=0, \quad \frac{\mathrm{d}^2u_0}{\mathrm{d}y^2}(1)=0, \quad \frac{\mathrm{d}^2u_1}{\mathrm{d}y^2}(1)=0,\\ &\theta_0(1)=1, \quad \theta_1(1)=0. \end{aligned} \tag{14}$$

Further, the heat transfer rate (Nusselt number) at both the walls is defined as [16]

$$Nu=A_4\left(\frac{\partial\theta}{\partial y}\right)_{y=0,1}.$$

Table 2. Comparison of present results with the results of Radhakrishnamacharya and Maiti [16] and the results obtained by NDSolve for $(\theta_0')_{y=0}$ for the Newtonian fluid case in the absence of nanoparticles, applied magnetic field, and thermal radiation.

Ec	$(\theta_0')_{y=0}$		
	Radhakrishnamacharya and Maiti [16]	Present results	NDSolve
1	0.233	0.231503510	0.231503491
2	0.308	0.305819915	0.305819919
5	0.531	0.528769134	0.528769167

Table 3. Comparison between the present results and NDSolve for heat transfer rate at $y = 0$ for different values of Ec, λ, and R when $R = 1$, $M = 2$, $Pr = 21$, $Ec = 0.6$, $Rd = 1$, $H = 2$, $\varepsilon = 0.001$, and $t = \pi$.

Parameter	Values	$A_4(\theta')_{y=0}$	
		Present results	NDSolve
Ec	0.0	0.010559977	0.010559951
	0.2	0.098651417	0.098653963
	0.4	0.186748076	0.186747976
λ	0.5	0.135699112	0.135699103
	1	0.075075830	0.075075312
	1.5	0.053645792	0.053645243
R	0.5	1.311751349	1.311757158
	1	0.274840147	0.274841989
	1.5	0.142813289	0.142813205

Now, Eqs. (10)–(13) with the appropriate BCs (14) are resolved by hiring the shooting technique with the support of the Runge–Kutta fourth-order procedure.

A comparison is made between the results obtained by present scheme with the results of Radhakrishnamacharya and Maiti [16] and with the results obtained by NDSolve for $(\theta_0')_{y=0}$ for the Newtonian fluid case in the absence of nanoparticles, applied magnetic field, and thermal radiation, which are presented in Table 2. The comparison shows that there is a good agreement between the present results, the results of Radhakrishnamacharya and Maiti [16], and the results obtained by NDSolve using MATHEMATICA software. Further, to check the correctness of the present results we made a comparison between the present results and the results obtained by NDSolve using MATHEMATICA, which are given in Table 3. It is observed that there is a good agreement between the present results and the results obtained by NDSolve.

4 Result and discussion

The current segment shows the impact of the emerging parameters on the temperature (θ), heat transfer rate (Nu), phase lag of temperature, and heat transfer rate of the Au + CuO-blood hybrid nanofluid with the help of pictorial presentations. For the current investigation, the considered values of various dimensionless parameters are $\lambda = 0.2$,

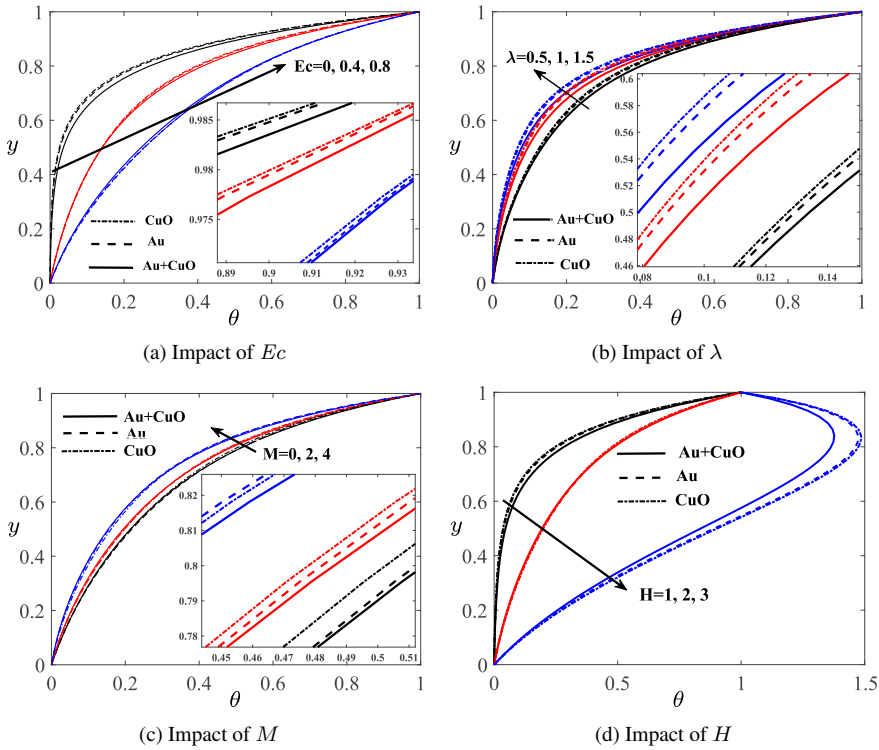

(a) Impact of Ec (b) Impact of λ

(c) Impact of M (d) Impact of H

Figure 2. Temperature distribution.

$M = 2$, $H = 2$, $R = 1$, $Rd = 1$, $Pr = 21$, $Ec = 0.6$, $Q = 1$, $t = \pi$, $\phi_{\text{Au}} = 0.05$, $\phi_{\text{CuO}} = 0.05$ unless otherwise stated. The graphical illustrations about the persuadence of Eckert number (Ec), Hartmann number (M), nanoparticles volume fractions, ϕ_{Au}, ϕ_{CuO}, couple stress parameter (λ), cross-flow Reynolds number (R), frequency parameter (H), radiation parameter (Rd), and the heat source/sink parameter (Q) on temperature, heat transfer rate, phase lag of temperature and heat transfer rate distributions of Au + CuO-blood hybrid nanofluid and the mono nanofluids Au-blood and CuO-blood are delineated in Figs. 2–6.

The impacts of Ec, λ, M, H, gold nanoparticles volume fraction (ϕ_{Au}) and copper oxide nanoparticles volume fraction (ϕ_{CuO}), R, Rd, and Q on temperature (θ) are depicted in Figs. 2(a)–2(d) and Figs. 3(a)–3(d). Figure 2(a) illustrates the physical behavior of temperature variations of conventional nanofluids and the hybrid nanofluid for uplifting values of Ec. It is found that for all cases of Au-blood, CuO-blood nanofluids, and Au + CuO-blood hybrid nanofluid, temperature profiles are increasing with an increment in Ec. Here the characterization of Ec dissipating the energy due to the internal friction of the nanoparticles, which is suspended in the blood. The temperature distribution of hybrid nanofluid is better than conventional nanofluids. Figure 2(b) displays the influence of couple stress parameter (λ) on the variation of temperature profiles of hybrid and

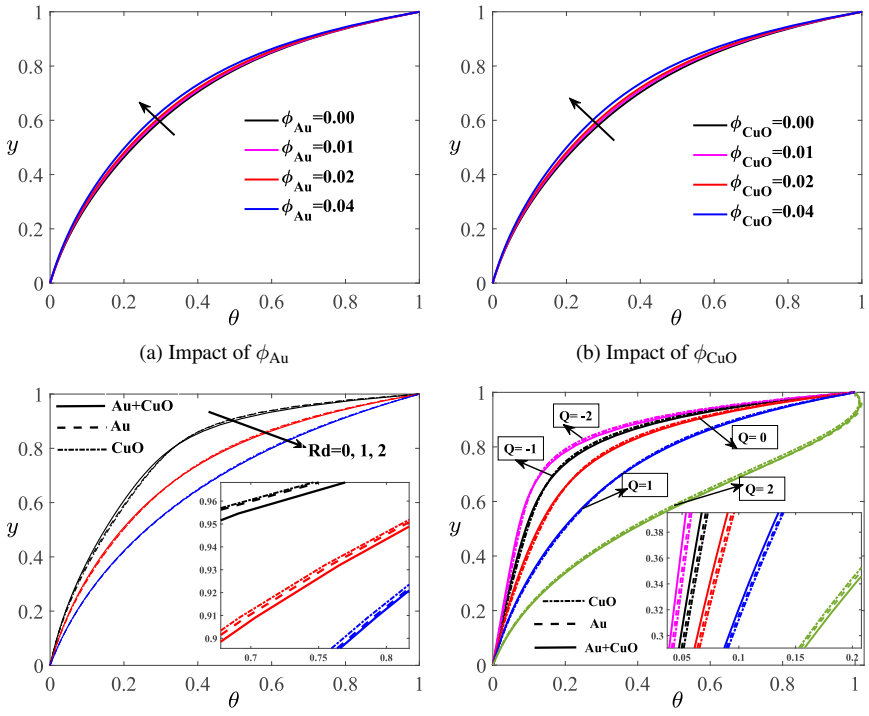

(a) Impact of ϕ_{Au} (b) Impact of ϕ_{CuO}

(c) Impact of Rd (d) Impact of Q

Figure 3. Temperature distribution.

conventional nanofluids. It reveals that there is a fall in the temperature with the rise of a couple stress parameter for the cases of hybrid and conventional nanofluids. From this figure one can see that Au + CuO-blood hybrid nanofluid has a significant influence on temperature variation than mono nanofluids Au-blood, CuO-blood. From Fig. 2(c) it is elucidated that the increasing Hartmann number retards the flow of electrically conducting couple stress hybrid nanofluid, which causes the decline in temperature distribution. From this one can infer that there is a fall in temperature with the high values of Hartmann number for all three cases. From the same figure it can be seen that the temperature distribution of hybrid nanofluid is greater than the conventional nanofluid near the suction wall, while it is lower near the injection wall. Figure 2(d) presents that for all three cases, there is a rise in temperature distribution with an increment in frequency parameter. The reason behind this is that increasing frequency parameter boost up the amplitude of the temperature.

From Figs. 3(a) and 3(b) one can understand that increasing volume fraction of nanoparticles Au, CuO lead to the deceleration in the temperature distribution. From Fig. 3(c) it is apparent that the raising of the radiation parameter increases the temperature of the current working fluid due to the radiation parameter has the relative commitment to the thermal transmission of conductive heat. Figure 3(d) displays the temperature distribution

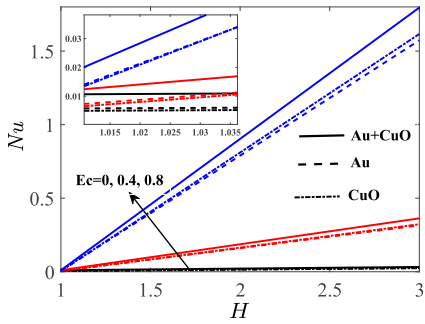

(a) Impact of Ec

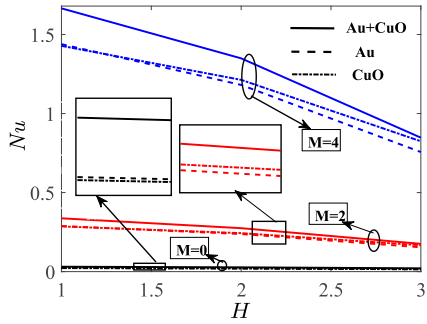

(b) Impact of M

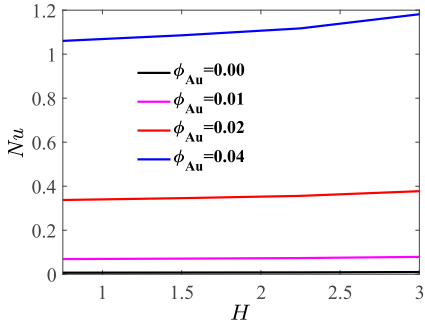

(c) Impact of ϕ_{Au}

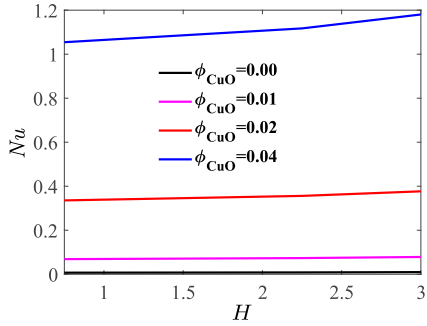

(d) Impact of ϕ_{CuO}

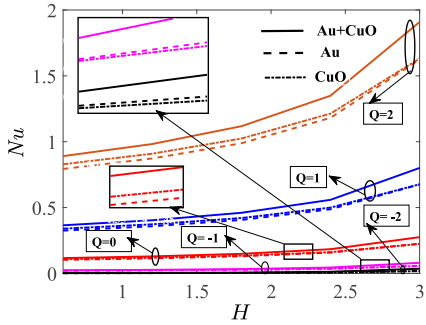

(e) Impact of Q

Figure 4. Heat transfer rate (Nu) against H.

for the cases of heat source and sink. Here the temperature is escalating for the uplifting values of the heat source ($Q > 0$), whereas the reverse behavior can be seen with an increasing values of the heat sink ($Q < 0$). Further, from Figs. 3(c) and 3(d) one can infer that the temperature distribution of hybrid nanofluid is better than the conventional nanofluid near the suction wall, while it is lower near the injection wall.

Figures 4(a)–4(e) are plotted to see the influence of emerging parameters Ec, M, gold nanoparticles volume fraction (ϕ_{Au}), copper oxide nanoparticles volume fraction (ϕ_{CuO}),

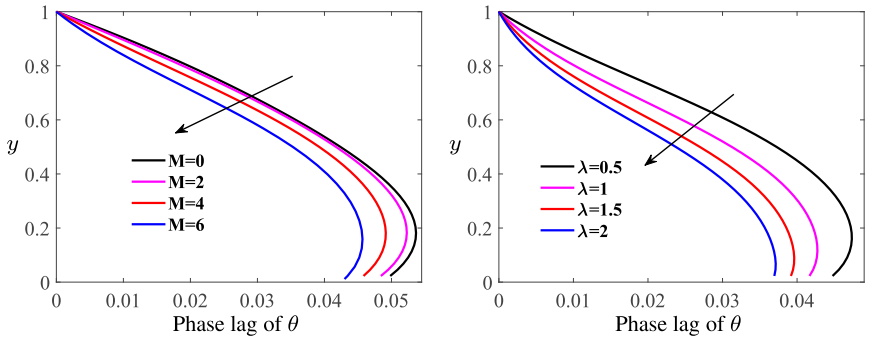

(a) Impact of M (b) Impact of λ

Figure 5. Phase lag of θ.

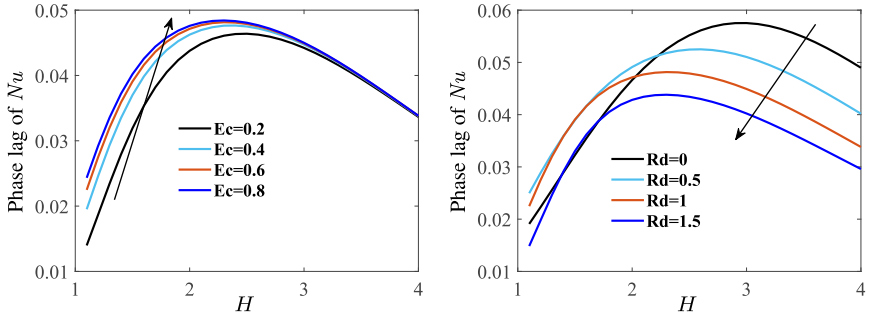

(a) Impact of Ec (b) Impact of Rd

Figure 6. Phase lag of Nu against H.

and Q on the heat transfer rate of hybrid and mono nanofluids against the frequency parameter at the lower wall $y = 0$. From these figures it is observed that the rate of heat transfer of hybrid nanofluid is higher than the heat transfer rate of conventional nanofluid. Figure 4(a) displays that the heat transfer rate is enhancing for various values of Eckert number, which is due to the increasing viscous dissipation escalating the rate of heat transfer. Figure 4(b) demonstrates that a rise in magnetic parameter increases the rate of heat transfer because of the retarding forces making the flow slowdown, which is created by the magnetic field. From Figures 4(c) and 4(d) it is portrayed that Nu is getting a boost up with the rising volume fractions of gold and copper oxide nanoparticles, thanks to the high thermal conductivity of the nanoparticles. Figure 4(e) illustrates that the heat transfer rate is increasing with an increment in the heat source, whereas the opposite behavior can be found for the higher values of the heat sink.

Figures 5(a)–5(b) display the variation of phase lag of the temperature of couple stress hybrid nanofluid for different values of Hartmann number and the couple stress parameter. From the same figures one can infer that phase lag decreases with increasing values of Hartmann number and couple stress parameter and the phase lag is maximum near to the

injection wall of the channel. The phase lag variation of heat transfer rate of couple stress hybrid nanofluid against the frequency parameter for the influences of Eckert number and the radiation parameter are displayed in Figs. 6(a)–6(b). Figure 6(a) shows that increasing viscous dissipation encouraging the phase lag of heat transfer rate and the maximum of the phase lag is near to the suction wall. Figure 6(b) elucidates that the maximum of phase lag of heat transfer rate is near to the suction wall of the channel, which is observed by increasing the thermal radiation.

5 Conclusion

In the current work, the hydromagnetic pulsatile flow of blood-based conducting couple stress hybrid nanofluid with the influences of Ohmic heating, heat source/sink, and thermal radiation has been discussed. The considered model is important in the study of biomedical engineering and nano-drug delivery. The numerical outcomes for dimensionless flow parameters are achieved by adopting the shooting method with the aid of the Runge–Kutta fourth-order scheme. The dynamics of blood flow is analyzed for hybrid nanofluid and conventional mono nanofluids. The main outcomes of the current analysis are summarized as follows:

- Temperature is raising for the magnifying Eckert number, whereas the reverse behavior can be found with a rise in couple stress parameter.
- An increment in volume fractions of gold and copper oxide nanoparticles decelerates the profiles of temperature distribution. The reverse trend can be seen with an escalation of radiation parameter.
- Temperature is increasing with the rising values of heat source and the increasing heat sink decreasing the temperature.
- The heat transfer rate is getting high with the high values of the Ec, and the same behavior is noticed with the uplifting magnetic field.
- The profiles of heat transfer rate distribution are increasing with a rise in volume fractions of gold and copper oxide nanoparticles.
- Phase lag of temperature is decreasing for the high values of M and λ. Phase lag of Nu is increasing with increasing values of Ec.

References

1. S.O. Adesanya, O.D. Makinde, Heat transfer to magnetohydrodynamic non-Newtonian couple stress pulsatile flow between two parallel porous plates, *Z. Naturforsch., A*, **67**:647–656, 2012, https://doi.org/10.5560/ZNA.2012-0073.
2. S. Ahmed, H. Xu, Forced convection with unsteady pulsating flow of a hybrid nanofluid in a microchannel in the presence of EDL, magnetic and thermal radiation effects, *Int. Commun. Heat Mass Transfer*, **120**:105042, 2021, https://doi.org/10.1016/j.icheatmasstransfer.2020.105042.

3. O.A. Alawi, N.A. Che Sidik, R. Mamat, Performance analysis of nanorefrigerants in heated and rotating concentric and eccentric annulus cylinders, *Jurnal Teknologi*, **77**:91–97, 2015, https://doi.org/10.11113/jt.v77.6159.
4. S.U.S. Choi, J.A. Eastman, Enhancing thermal conductivity of fluids with nanoparticles, *Am. Soc. Mech. Eng. Fluids Eng. Div, FED, Vol. 231*, pp. 99–105, 1995, https://www.osti.gov/servlets/purl/196525.
5. Y.S. Daniel, Z.A. Aziz, Z. Ismail, F. Salah, Effects of thermal radiation, viscous and Joule heating on electrical MHD nanofluid with double stratification, *Chin. J. Phys.*, **55**:630–651, 2017, https://doi.org/10.1016/j.cjph.2017.04.001.
6. M. Devakar, T.K.V. Iyengar, Stokes' problems for an incompressible couple stress fluid, *Nonlinear Anal. Model. Control*, **13**(2):181–190, 2008, https://doi.org/10.15388/NA.2008.13.2.14578.
7. S.P.A. Devi, S.S.U. Devi, Numerical investigation of hydromagnetic hybrid $Cu - Al_2O_3$/water nanofluid flow over a permeable stretching sheet with suction, *Int. J. Nonlinear Sci. Numer. Simul.*, **17**:249–257, 2016, https://doi.org/10.1515/ijnsns-2016-0037.
8. M.M. Hashmi, T. Hayat, A. Alsaedi, On the analytic solutions for squeezing flow of nanofluid between parallel disks, *Nonlinear Anal. Model. Control.*, **17**:418–430, 2012, https://doi.org/10.15388/na.17.4.14048.
9. M. Hatami, J. Hatami, D.D. Ganji, Computer simulation of MHD blood conveying gold nanoparticles as a third grade non-Newtonian nanofluid in a hollow porous vessel, *Comput. Methods Programs Biomed.*, **113**:632–641, 2014, https://doi.org/10.1016/j.cmpb.2013.11.001.
10. S. Hussain, S.E. Ahmed, T. Akbar, Entropy generation analysis in MHD mixed convection of hybrid nanofluid in an open cavity with a horizontal channel containing an adiabatic obstacle, *Int. J. Heat Mass Transfer*, **114**:1054–1066, 2017, https://doi.org/10.1016/j.ijheatmasstransfer.2017.06.135.
11. M. Jawad, A. Khan, S.A.A. Shah, Examination of couple stress hybrid nanoparticles (CuO-Cu/blood) as a targeted drug carrier with magnetic effects through porous sheet, *Braz. J. Phys.*, **51**(4):1096–1107, 2021, https://doi.org/10.1007/s13538-021-00930-7.
12. M.E.M. Khedr, A.J. Chamkha, M. Bayomi, MHD flow of a micropolar fluid past a stretched permeable surface with heat generation or absorption, *Nonlinear Anal. Model. Control*, **14**(1):27–40, 2009, https://doi.org/10.15388/NA.2009.14.1.14528.
13. C.K. Kumar, S. Srinivas, A.S. Reddy, MHD pulsating flow of Casson nanofluid in a vertical porous space with thermal radiation and Joule heating, *J. Mech.*, **36**:535–549, 2020, https://doi.org/10.1017/jmech.2020.5.
14. M. Muneeshwaran, G. Srinivasan, P. Muthukumar, C.C. Wang, Role of hybrid-nanofluid in heat transfer enhancement – A review, *Int. Commun. Heat Mass Transfer*, **125**:105341, 2021, https://doi.org/10.1016/j.icheatmasstransfer.2021.105341.
15. M.E. Qomi, G.A. Sheikhzadeh, A. Fattahi, Heat transfer enhancement in a microchannel using a pulsating MHD hybrid nanofluid flow, *Energy Sources, Part A*, 2020, https://doi.org/10.1080/15567036.2020.1834031.
16. G. Radhakrishnamacharya, M.K. Maiti, Heat transfer to pulsatile flow in a porous channel, *Int. J. Heat Mass Transfer*, **20**(2):171–173, 1977, https://doi.org/10.1016/0017-9310(77)90009-6.

17. S. Rajamani, A.S. Reddy, Pulsating flow of electrically conducting couple stress nanofluid in a channel with ohmic dissipation and thermal radiation – Dynamics of blood, *Proc. Inst. Mech. Eng., Part E, J. Process Mech. Eng.*, **235**(6):1895–1909, 2021, https://doi.org/10.1177/09544089211025177.

18. J. Rana, P.V.S.N. Murthy, Solute dispersion in pulsatile Casson fluid flow in a tube with wall absorption, *J. Fluid Mech.*, **793**:877–914, 2016, https://doi.org/10.1017/jfm.2016.155.

19. A.S. Reddy, S. Srinivas, K. Jagadeshkumar, Blood-gold/coppernanofluid flow between expanding or contracting permeable walls with slip effects, *Mater. Today Proc.*, **9**:351–360, 2019, https://doi.org/10.1016/j.matpr.2019.02.164.

20. M.U. Sajid, H.M. Ali, Thermal conductivity of hybrid nanofluids: A critical review, *Int. J. Heat Mass Transfer*, **126**:211–234, 2018, https://doi.org/10.1016/j.ijheatmasstransfer.2018.05.021.

21. D.S. Sankar, Perturbation analysis for pulsatile flow of Carreau fluid through tapered stenotic arteries, *Int. J. Biomath.*, **9**:1–25, 2016, https://doi.org/10.1142/S1793524516500637.

22. J. Sarkar, P. Ghosh, A. Adil, A review on hybrid nanofluids: Recent research, development and applications, *Renewable and Sustainable Energy Rev.*, **43**:164–177, 2015, https://doi.org/10.1016/j.rser.2014.11.023.

23. H.M. Shawky, Pulsatile flow with heat transfer of dusty magnetohydrodynamic Ree-Eyring fluid through a channel, *Heat Mass Transfer*, **45**(10):1261–1269, 2009, https://doi.org/10.1007/s00231-009-0502-0.

24. P. Sreedevi, P.S. Reddy, A. Chamkha, Heat and mass transfer analysis of unsteady hybrid nanofluid flow over a stretching sheet with thermal radiation, *SN Appl. Sci.*, **2**, 2020, https://doi.org/10.1007/s42452-020-3011-x.

25. S. Srinivas, C.K. Kumar, A.S. Reddy, Pulsating flow of Casson fluid in a porous channel with thermal radiation, chemical reaction and applied magnetic field, *Nonlinear Anal. Model. Control*, **23**:213–233, 2018, https://doi.org/10.15388/NA.2018.2.5.

26. D. Srinivasacharya, D. Srikanth, Effect of couple stresses on the pulsatile flow through a constricted annulus, *C. R., Méc., Acad. Sci. Paris*, **336**(11):820–827, 2008, https://doi.org/10.1016/j.crme.2008.09.008.

27. V.K. Stokes, Effects of couple stresses in fluids on hydromagnetic channel flows, *Phys. Fluids*, **11**:1131–1132, 1984, https://doi.org/10.1063/1.1692056.

28. D. Tripathi, J. Prakash, M.G. Reddy, R. Kumar, Numerical study of electroosmosis-induced alterations in peristaltic pumping of couple stress hybrid nanofluids through microchannel, *Indian J. Phys.*, **95**:2411–2421, 2021, https://doi.org/10.1007/s12648-020-01906-0.

29. G. Venkatesan, A.S. Reddy, Insight into the dynamics of blood conveying alumina nanoparticles subject to Lorentz force, viscous dissipation, thermal radiation, Joule heating, and heat source, *Eur. Phys. J. Spec. Top.*, **230**(5):1475–1485, 2021, https://doi.org/10.1140/epjs/s11734-021-00052-w.

30. A. Vijayalakshmi, S. Srinivas, B. Satyanarayana, A. Subramanyam Reddy, Hydromagnetic pulsating flow of nanofluid between two parallel walls with porous medium, *Mater. Today Proc.*, **9**:306–319, 2019, https://doi.org/10.1016/j.matpr.2019.02.161.

31. C.Y. Wang, Pulsatile flow in a porous channel, *J. Appl. Mech.*, **38**:553–555, 1971, https://doi.org/10.1115/1.3408822.

32. Q. Ye, Y. Zhang, J. Wei, A comprehensive review of pulsating flow on heat transfer enhancement, *Appl. Therm. Eng.*, **196**:117275, 2021, https://doi.org/10.1016/j.applthermaleng.2021.117275.

33. A. Zaib, S. Shafie, Thermal diffusion and diffusion thermo effects on unsteady MHD free convection flow over a stretching surface considering Joule heating and viscous dissipation with thermal stratification, chemical reaction and Hall current, *J. Franklin Inst.*, **351**:1268–1287, 2014, https://doi.org/10.1016/j.jfranklin.2013.10.011.